

Electrochemical Model Parameter Identification of Lithium-Ion Battery with Temperature and Current Dependence

Long Chen¹, Ruyu Xu¹, Weining Rao¹, Huanhuan Li^{1,3*}, Ya-Ping Wang^{2,3}, Tao Yang⁴, Hao-Bin Jiang¹

¹ Automotive Engineering Research Institute, Jiangsu University, 301 Xuefu Road, Zhenjiang 212013, P. R. China

² School of Material Science & Engineering, Jiangsu University, Zhenjiang 212013, P. R. China

³ Key Laboratory of Advanced Energy Materials Chemistry (Ministry of Education), College of Chemistry, Nankai University, Tianjin 300071, China

⁴ Jiangsu Chunlan Clean Energy Research Institute Co., Ltd., 73 Beichang Road, Taizhou, 225300, P. R. China

*E-mail: lihh@mail.ujs.edu.cn

Received: 8 January 2019 / Accepted: 14 February 2019 / Published: 10 April 2019

Battery modelling and state estimation are crucial for lithium-ion batteries applied in electrical vehicles (EVs). In this work, a simplified electrode-average electrochemical model of a lithium-ion battery that adopts a polynomial approximation and a three-variable method to reduce the order of the solid and electrolyte phase diffusion equations is designed. A novel parameter identification method considering temperature and current is also proposed to reduce the parameter deviation caused by different working conditions. The model parameters are identified by the genetic algorithm (GA) offline at different temperatures and currents to create lookup tables for online estimation. Furthermore, 3.5 Ah NCM 18650-type cells are chosen to validate the simplified model and the proposed estimation method. The results indicate that the proposed scheme is accurate, simple and flexible for current and temperature changes under different operation conditions.

Keywords: Lithium-ion battery, Model simplification, Parameter identification, Temperature and current uncertainties

1. INTRODUCTION

Electric vehicles, including hybrid electric vehicles (HEVs), plug-in hybrid electric vehicles (PHEVs) and pure electric vehicles (PEVs), have been widely developed due to the explosion of the energy crisis and global warming. Recently, compared with other batteries, lithium-ion batteries (LIBs) have been widely utilized not only for their high density, high power density, long cycle life and environmental friendliness [1] but also for their low self-discharge rate and lack of a memory effect [2].

Reliability and safety issues coupled with the abovementioned advantages are challenging and crucial for LIBs, especially under extreme conditions. To address this problem, a battery management system (BMS) was proposed to monitor and protect the battery, which can not only prevent it from over-charge/discharge and explosion under extreme temperature but also optimize battery performance, extend cycle life and increase driving range. In the design of a BMS, the cell voltage and the operating states efficiently estimated are key issues. The battery states, including state of charge (SOC), state of health (SOH) and state of function (SOF), cannot be directly evaluated [1]. Accordingly, various battery models are employed to estimate these operating states, which are closely dependent on the related battery parameters. Thus, model parameter identification is indispensable and critical for BMS design.

A considerable number of researchers have investigated battery models and presented numerous effective methods for parameter identification. The models of LIBs mainly cover equivalent circuit models (ECMs) and electrochemical models [3]. Electrochemical models are able to describe the internal reactions of batteries, including intercalation/deintercalation of Li^+ in electrode materials via three transport phenomena (migration, diffusion and convection). Convection is normally neglected in battery modelling due to its weak effect [4]. Two of the most widely used and studied electrochemical models are the pseudo-two-dimensional (P2D) model and the single particle model (SPM). The P2D model is described by several highly nonlinear partial differential equations (PDEs) based on porous electrode theory, concentrated solution theory and kinetics equations [5, 6]. There are different simplified versions of the P2D model due to its complexity, such as the parabolic profile approximation model [7], electrode averaged model (EAM) [8] and proper orthogonal decomposition (POD) model [9]. The SPM was proposed by approximating both positive and negative electrodes as two spherical particles and neglecting the concentration of Li^+ in the liquid phase, which greatly improves the calculation speed of the model and offers good accuracy at a low current rate. In our previous work, an extended single-particle (ESP) electrochemical model was established based on the SPM by considering the influence of the electrolyte phase potential on the battery terminal voltage, which improves the accuracy of the SPM under high-magnification-current conditions [10]. Generally, the more the model is simplified, the less computational time it needs, but the lower its accuracy is. Compared with the equivalent circuit models, the electrochemical models are more accurate and can capture important dynamics, including solid-phase diffusion, at the expense of computational resources, but they are more sophisticated and unsuitable for online applications. Thus, it is crucial to balance model fidelity and computational burden to satisfy different application requirements.

Furthermore, the accuracy of the model used is closely related to parameter identification. Currently, researchers have suggested many effective methods to improve the accuracy of parameter identification, such as various Kalman filters methods, least-squares methods and evolutionary computation technology. In general, the electrical parameters depend on several variables, including temperature, SOC, current and ageing [11, 12]. Yuan et al. utilized the recursive least-squares algorithm to estimate simplified electrochemical model parameters by establishing the parameter relationship between an equivalent circuit model and a simplified electrochemical model [13]. The new method improves the comprehension level of the two models. Shen et al. [14] proposed a particle swarm optimization and Levenberg-Marquardt (PSO-LM) algorithm to realize the multi-scale parameter identification of LIBs, which accelerates the convergence rate and resolves the local minimum

entrapment drawback but increases the computational cost. Compared with the abovementioned methods, the genetic algorithm (GA) [15], as a parameter identification method, is frequently used to identify nondestructive parameters because of its flexibility for different objective functions, excellent optimization performance even with unknown initial parameters and good algorithm convergence. However, the algorithm’s drawbacks limit its application, including long computational processes and repeated calculations [16]. To tackle this problem, the simplified model parameters are estimated by the GA offline and change with the current and temperature for application in BMS and embedded systems.

In this work, a simplified electrode-average model with a solid-phase diffusion equation reduced by polynomial approximation and a three-variable method is proposed, which not only captures the dynamic behaviour of the battery but also simplifies the physics-based equations expressing concentration transport and conservation of charge for the solid and electrolyte phases to reduce the model’s complexity. Furthermore, a novel parameter estimation method is developed, in which the nonlinear model parameters are identified by the GA offline from measured data directly, then applied to lookup tables and varied with real-time current and outside temperature. The simplified model with estimated parameters applied can simulate battery behaviours under different operation conditions steadily and efficiently. To validate the simplified model and the proposed estimation method, 3.5 Ah NCM 18650-type cells are selected. The experiments include constant current discharge tests and two self-designed pulse current tests.

2. MODEL DEVELOPMENT

2.1. Model simplification

2.1.1. Electrochemical mechanism

The electrochemical model of LIBs based on chemical/electrochemical kinetics and transport equations is utilized to simulate the electrochemical phenomena and characteristics.

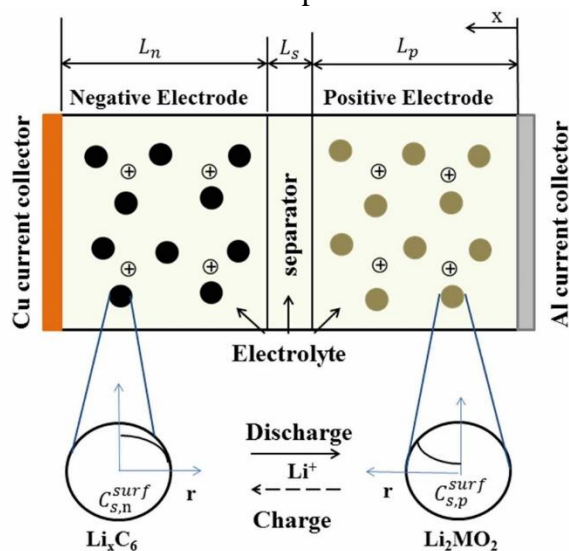


Figure 1. Schematic diagram of the P2D model of the lithium-ion battery.

Figure 1 is a schematic diagram of the lithium-ion battery model, which consists of a positive electrode, a negative electrode, a separator and an electrolyte, and the two dimensions are the radial dimension in the porous spherical particles and the dimension x along the thickness. The cathode material (NCM) and anode material (graphite) are smeared on aluminium (Al) and copper (Cu) foil current collectors, respectively. During discharge, the Li^+ de-intercalating from the anode passes through the separator and intercalates into the cathode. The opposite process occurs during charge.

2.1.2. Electrode average model simplification

The electrode-average model proposed by Domenico et al. [8] couples multiple partial differential equations (PDEs) to describe the internal electrochemical reactions of LIBs in detail. The average model is based on two assumptions: the concentration of Li^+ in the electrolyte is constant, and the solid concentration distribution along the electrode is negligible. To satisfy the embedded control system and estimation application, the simplified model loses partial information pertaining to LIBs, but it can reduce computational complexity and capture crucial dynamic characteristics. The governing equations and boundary conditions are introduced briefly as follows.

The concentration of Li^+ in solid-phase particles is described by Fick's diffusion law:

$$\frac{\partial C_s(x, r, t)}{\partial t} = \frac{D_s}{r^2} \frac{\partial}{\partial r} \left(r^2 \frac{\partial C_s(x, r, t)}{\partial r} \right) \tag{1}$$

The boundary conditions are as follows:

$$\left. \frac{\partial C_s(x, r, t)}{\partial r} \right|_{r=0} = 0 \tag{2}$$

$$D_s \left. \frac{\partial C_s(x, r, t)}{\partial r} \right|_{r=R_s} = -\frac{j(x, t)}{a_s F} \tag{3}$$

where the specific surface area of the porous electrode is $a_{s,i} = \frac{3\varepsilon_{s,i}}{R_i}$, $i = p, n$.

The concentration of charge in the solid phase of the two electrodes is governed by Ohm's law:

$$\sigma_e \text{ff} \frac{\partial^2 \phi_s(x, t)}{\partial x^2} = j(x, t) \tag{4}$$

The corresponding boundary conditions are as follows:

$$-\sigma_{\text{eff},p} \left. \frac{\partial \phi_{s,p}}{\partial x} \right|_{x=0} = -\sigma_{\text{eff},n} \left. \frac{\partial \phi_{s,n}}{\partial x} \right|_{x=L} = \frac{I(t)}{A} \tag{5}$$

$$-\sigma_{\text{eff},p} \left. \frac{\partial \phi_{s,p}}{\partial x} \right|_{x=L_p} = -\sigma_{\text{eff},n} \left. \frac{\partial \phi_{s,n}}{\partial x} \right|_{x=L_p+L_s} = 0 \tag{6}$$

The concentration of charge in the electrolyte is

$$\frac{\partial}{\partial x} \left(K^{\text{eff}} \frac{\partial}{\partial x} \phi_e(x, t) \right) + \frac{\partial}{\partial x} \left(\frac{K_D^{\text{eff}}}{C_{e,0}} \frac{\partial}{\partial x} C_e(x, t) \right) + j(x, t) = 0 \tag{7}$$

$$K_D^{\text{eff}} = \frac{-2RT}{F} K^{\text{eff}} (1 - t_+^0) \left(1 + \frac{d \ln f_{\pm}}{d \ln C_e} \right) \tag{8}$$

where the effective electrolyte conductivity $K^{eff} = K \varepsilon_e^{brug}$, $brug = 1.5$, with the following boundary conditions:

$$\left. \frac{\partial \phi_e(x,t)}{\partial x} \right|_{x=0} = \left. \frac{\partial \phi_e(x,t)}{\partial x} \right|_{x=L} = 0 \tag{9}$$

The electrochemical reaction kinetics are described by the Butler-Volmer equation:

$$i(x,t) = a_s i_0 \left\{ \exp\left(\frac{\alpha_a F}{RT} \eta\right) - \exp\left(-\frac{\alpha_c F}{RT} \eta\right) \right\} \tag{10}$$

$$i_0 = k(C_e)^{\alpha_a} (C_{s,max} - C_{s,surf})^{\alpha_a} (C_{s,surf})^{\alpha_c} \tag{11}$$

A constant value \bar{j} is used to replace Butler-Volmer current j because of the average solid concentration. Equation (12) is derived from integrating equation (4) with the boundary conditions (5) and (6) applied.

$$\int j(x) dx = \frac{I}{A} = \bar{j}L \tag{12}$$

The Butler-Volmer current of the negative and positive electrodes are

$$j_n = \bar{j}_n = \frac{I}{AL_n} \tag{13}$$

$$j_p = \bar{j}_p = \frac{I}{AL_p} \tag{14}$$

The potential caused by electrolyte phase impedance is considered, and the influence of the concentration of Li^+ in the electrolyte is neglected. Combining equations (7) – (9), the electrolyte phase potential difference is

$$\overline{\phi_{e,p}} - \overline{\phi_{e,n}} = \phi(L) - \phi(0) = -\frac{I}{2A} \left(\frac{L_n}{K_n^{eff}} + \frac{2L_s}{K_s^{eff}} + \frac{L_p}{K_p^{eff}} \right) \tag{15}$$

To obtain the overpotential, the Butler-Volmer equation can be rewritten as

$$j(x,t) = \frac{1}{2} a_s i_0 \sinh\left(\frac{0.5F}{RT} \eta\right) \tag{16}$$

where $\sinh\left(\frac{0.5F}{RT} \eta\right) = \frac{2j(x,t)}{a_s i_0} = \xi$, and the overpotential equation can be expressed as

$$\eta = \frac{RT}{0.5F} \ln\left(\xi + \sqrt{\xi^2 + 1}\right) \tag{17}$$

The concentration of Li^+ in the solid phase is governed by Fick's diffusion law, and the curve of the surface concentration of Li^+ in spherical particles resembles a parabola during charge and discharge, as shown in Figure 1. To simplify equation (1) and realize model reduction, the polynomial approximation and a three-variable model suggested by Thanh-Son Dao et al. [17] are chosen.

The concentration of Li^+ in the solid phase can be expressed as

$$C_s(t,r) = a(t) + b(t) \frac{r^2}{R_i^2} + c(t) \frac{r^4}{R_i^4} \tag{18}$$

Three coefficients are obtained by substituting equation (18) into equation (1) considering the surface concentration of Li^+ in the solid phase $C_{s,surf}(t)$, the average concentration of Li^+ in the solid phase

$\bar{C}_s(t)$ and the volume-averaged concentration flux $\bar{q}(t)$ (for the detailed solution, see Subramanian et al. [18]).

$$a(t) = \frac{39}{4} C_{s,surf}(t) - \frac{35}{4} \bar{C}_s(t) - 3\bar{q}(t) R_i \tag{19}$$

$$b(t) = -35 C_{s,surf}(t) + 35 \bar{C}_s(t) + 10\bar{q}(t) R_i \tag{20}$$

$$c(t) = \frac{105}{4} C_{s,surf}(t) - \frac{105}{4} \bar{C}_s(t) - 7\bar{q}(t) R_i \tag{21}$$

Equation (1) can be reduced to the following two ordinary differential equations (ODEs) by substituting equations (19)-(20) into equation (18).

$$\frac{d}{dt} \bar{q}(t) + 30 \frac{D_s}{R_i^2} \bar{q}(t) + \frac{45}{2} \frac{J(t)}{R_i^2} = 0 \tag{22}$$

$$\frac{dC_{s,surf}(t)}{dt} = -\frac{57}{7} \frac{J(t)}{R_i} - \frac{48D_s}{7R_i} \bar{q}(t) \tag{23}$$

where the wall flux of Li^+ on an intercalation particle of the electrode is $J(t) = \frac{j(t)}{a_s F}$.

An average model reduced with a three-variable approximation applied in the solid phase is realized, and the cell output voltage is described as

$$V_i = U_p - U_n + \eta_p - \eta_n + \overline{\phi_{e,p}} - \overline{\phi_{e,n}} - R_f I = U_p - U_n + \frac{RT}{\alpha_n} \ln \frac{\xi_p + \sqrt{\xi_p^2 + 1}}{\xi_n + \sqrt{\xi_n^2 + 1}} - \frac{I}{2A} \left(\frac{L_n}{K_n^{eff}} + \frac{2L_s}{K_s^{eff}} + \frac{L_p}{K_p^{eff}} \right) - R_f I \tag{24}$$

In equation (24), U_p and U_n are the open-circuit voltages (OCVs) of the positive and negative electrodes, respectively. The positive equilibrium U_p is formulated as in reference [19], whose cathode material NCM is the same as that in the test cell.

$$U_p = (-4.875 + 5.839 * \theta_p - 1.507 * \theta_p^3 + 0.531 * \theta_p^5) / (\theta_p - 1.005) \tag{25}$$

The negative equilibrium U_n is obtained by curve fitting.

$$U_n = -104.4 * \theta_n^5 + 217.3 * \theta_n^4 - 169 * \theta_n^3 + 61.79 * \theta_n^2 - 11.43 * \theta_n + 1.234 \tag{26}$$

where the electrode-level state of charge θ_i is defined as follows:

$$\theta_i = \frac{C_{s,i}^{surf}}{C_{s,i,max}}, (i = p, n) \tag{27}$$

The simplified average model is programmed and simulated in the MATLAB/SIMULINK platform, and the next step is to estimate the related model parameters.

2.2. Parameter identification

2.2.1. Electrochemical model parameters

The electrochemical model describes complex internal electrochemical reactions of LIBs and has numerous parameters, which are difficult to estimate by experimental measurement directly. Table 1

shows most of the model parameters of the 3.5 Ah 18650-type NCM cells that we chose. The cell structure parameters are derived from reference [19], such as the thickness and particle radius. The other parameters are adopted from references [20-22]. Otherwise, seven model parameters ($D_{s,n}$, $D_{s,p}$, $\varepsilon_{e,n}$, $\varepsilon_{e,p}$, $\varepsilon_{e,s}$, $\varepsilon_{s,n}$ and $\varepsilon_{s,p}$) are identified by the GA with temperature and current changes considered because these parameters usually change with cell type and are closely associated with battery characteristics.

Table 1. Parameters for the electrochemical model of the LIBs

Parameters	Negative electrode	Separator	Positive electrode
L/cm	8.1×10^{-3}	2×10^{-3}	7.8×10^{-3}
R_s /cm	1×10^{-3}	-	5×10^{-4}
θ_0	0.126	-	0.870
θ_{100}	0.676	-	0.442
$C_{s,max}$ /(mol·cm ⁻³)	0.0306	-	0.0516
k/(A·cm ^{2.5} ·mol ^{-1.5})	9.6487×10^{-11}	-	2.89461×10^{-11}
C_e /mol·cm ⁻³)		1.2×10^{-3}	
R/(J·mol ⁻¹)		8.314	
K/(S·cm)	$0.0911 + 1.9101 \times 10^{-3} C_e$	$-1.052 \times 10^{-6} C_e^2 + 0.1554 \times 10^{-9} C_e^3$	
F/(C·mol ⁻¹)		96485	
R_f/Ω		0.028	
A/m ²		0.2	
$\alpha_a = \alpha_c$		0.5	

2.2.2. Offline and online estimation

The effects of temperature and current are considered because they are closely related to battery characteristics and change with the external environment and driving conditions. Figure 2 shows the temperature rise of 3.5 Ah NCM 18650-type cells in a programmable fast thermal test chamber set to 20°C at a current of 0.2, 0.5, 1 and 2C, respectively. The test details are introduced in the first paragraph of section 3.1. *Experimental verification*, and their maximal temperature increases are exhibited in Table 2. As shown in Figure 2, the temperature rise of the cell increases as the current increases, especially at the end of discharge. The temperature rises gently and slightly below the 1C discharge current rate but rapidly and drastically above 2C, for which the maximal temperature rise reaches 14.8°C at 2C. Therefore, parameter identification involves two processes: utilizing 2-D lookup tables to estimate parameters online for discharge current rates below 1C based on the prepared parameters identified by GA, and applying the GA to estimate parameters directly for high current with increasing temperature. Compared with a coupled electrochemical-thermal model that can also describe the temperature effect, the proposed method based on the simplified model is less complex, incurs a lower computational cost and is more suitable for online applications.

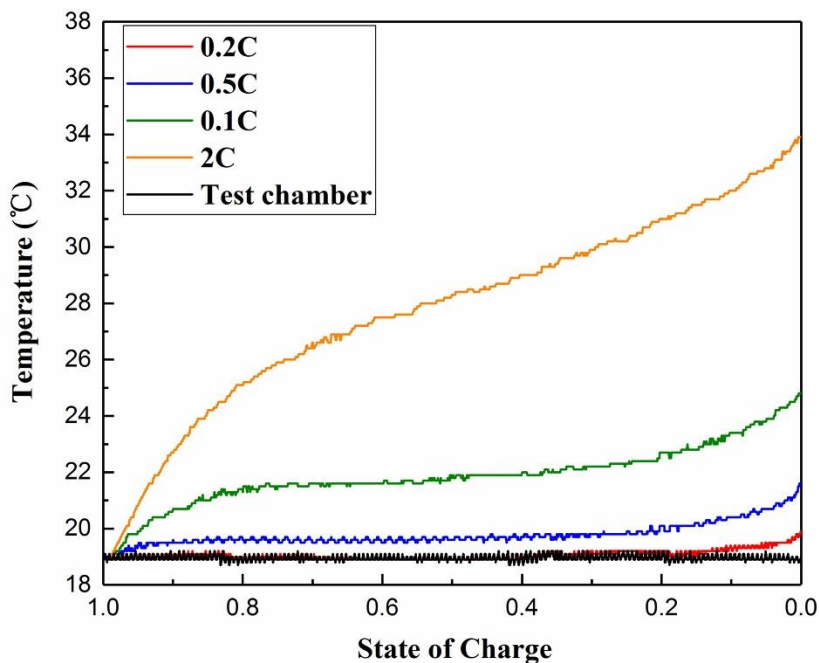


Figure 2. Temperature increases of cells at different current rates of 0.2, 0.5, 1 and 2C.

Table 2. Maximal temperature increase of cells under different current rates.

Current rate	0.2	0.5	1	2
Rise (°C)	0.9	2.4	5.6	14.8

The GA is a global optimization probabilistic search algorithm modelled after natural evolution. During each evolution process, new individuals are generated by fitness-proportionate selection, and randomly selected crossover and mutation operations are applied to the genes of individuals [22]. The GA was applied to estimate the seven unknown parameters offline with the temperature and current considered; the corresponding flow chart is shown in Figure 3. Each GA individual includes 7 variables: $D_{s,n}$, $D_{s,p}$, $\epsilon_{e,n}$, $\epsilon_{e,p}$, $\epsilon_{e,s}$, $\epsilon_{s,n}$ and $\epsilon_{s,p}$ respectively. Table 3 shows the value ranges of the seven parameters. The population size, number of genetic iterations, crossover probability P_c and mutation probability P_m in the GA are set to 50, 100, 0.6 and 0.007, respectively. Furthermore, the following fitness function (28) of individuals is the sum of the squares of the output voltage errors between the simplified model and tested cells. The GA process is repeated at each temperature (10°C, 20°C, 30°C and 40°C) and each discharge current rate (0.2C, 0.5C, 1C and 2C) based on the collected experimental data, and the estimated results are listed in Table 4. From Figure 2, the temperature rise of 1C is below 3°C when the SOC is as low as 0.2; therefore, the estimated results of discharge current rate (<1C) at different temperatures can be considered the true values of the corresponding temperature and prepared for lookup tables. However, the parameters associated with a discharge current rate of 2C should be estimated by the GA directly offline at different temperatures because of the drastic increase in temperature.

$$f = \sum_0^{t-1} (U_{sim} - U_{exp})^2 \tag{28}$$

Table 3. Value ranges of the parameters

$D_{s,n}$	$D_{s,p}$	$\epsilon_{e,n}$	$\epsilon_{e,p}$	$\epsilon_{e,s}$	$\epsilon_{s,n}$	$\epsilon_{s,p}$
$1 \times 10^{-12} \sim 1 \times 10^{-9}$	$1 \times 10^{-12} \sim 1 \times 10^{-9}$	0~0.9	0~0.9	0~0.9	0~0.9	0~0.9

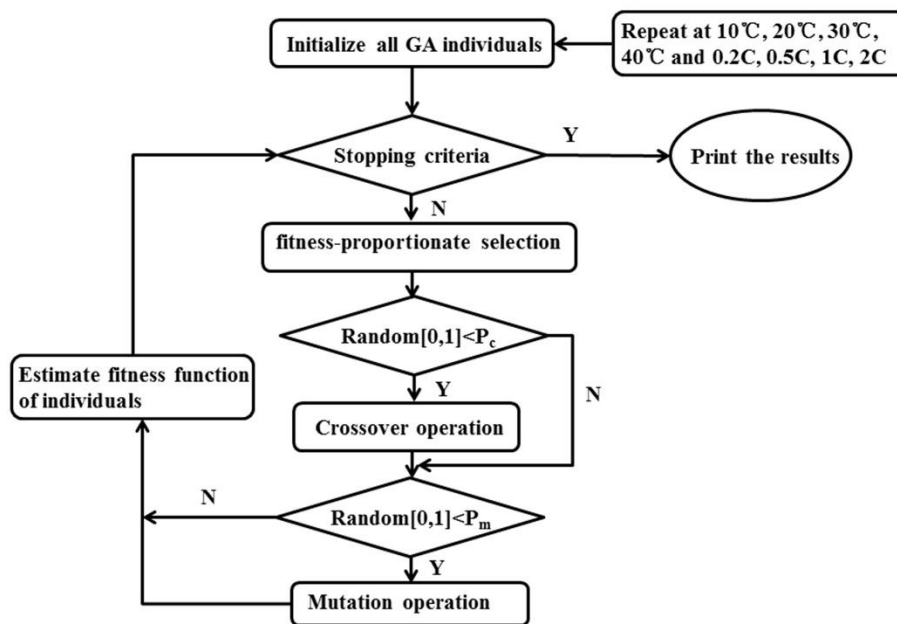


Figure 3. The flow diagram of the GA for offline parameter identification.

Table 4. Estimated model parameters related to discharge current rate and temperature.

Current rate	Temperature /°C	$D_{s,n}$	$D_{s,p}$	$\epsilon_{e,n}$	$\epsilon_{e,p}$	$\epsilon_{e,s}$	$\epsilon_{s,n}$	$\epsilon_{s,p}$
0.2C	10	1.6436×10^{-10}	1.8022×10^{-11}	0.035027	0.035027	0.035027	0.37529	0.27293
	20	3.9277×10^{-11}	1.0334×10^{-11}	0.20493	0.20493	0.20493	0.4052	0.29265
	30	1.842×10^{-11}	1.4263×10^{-11}	0.89367	0.89367	0.89367	0.46286	0.30718
	40	2.735×10^{-11}	4.0012×10^{-11}	0.89936	0.89936	0.89936	0.42979	0.28462
0.5C	10	1.0762×10^{-10}	4.5105×10^{-11}	0.037796	0.037796	0.037796	0.38256	0.26876
	20	5.5322×10^{-11}	3.3813×10^{-11}	0.055918	0.055918	0.055918	0.43362	0.28891
	30	4.5222×10^{-11}	4.2143×10^{-11}	0.088903	0.088903	0.088903	0.45054	0.29052
	40	3.9448×10^{-11}	4.267×10^{-11}	0.1512	0.1512	0.1512	0.46315	0.29245
1C	10	2.2327×10^{-10}	9.9984×10^{-10}	0.039019	0.039019	0.039019	0.37125	0.27957
	20	1.7845×10^{-10}	1.0226×10^{-12}	0.072594	0.072594	0.072594	0.40594	0.66471
	30	7.1675×10^{-11}	9.8954×10^{-10}	0.069648	0.069648	0.069648	0.46713	0.27768
	40	5.4504×10^{-11}	2.038×10^{-10}	0.094308	0.094308	0.094308	0.4983	0.28369
2C	10	4.4473×10^{-10}	9.9995×10^{-10}	0.048197	0.048197	0.048197	0.38235	0.29589
	20	2.7963×10^{-11}	9.6593×10^{-10}	0.043899	0.043899	0.043899	0.66623	0.30304
	30	5.4083×10^{-11}	9.9942×10^{-10}	0.078452	0.078452	0.078452	0.59951	0.28355
	40	6.268×10^{-11}	9.9987×10^{-10}	0.095161	0.095161	0.095161	0.57771	0.28204

A 2-D lookup table based on the results estimated by the GA is utilized to describe the relationship between each parameter and the corresponding temperature/ discharge current rate ($<1C$) to realize real-time estimation because of the approach's accuracy and celerity [23]. Each parameter of the model is a function of temperature T and discharge current rate C .

$$D_{s,n} = D_{s,n}(T, C)$$

$$D_{s,p} = D_{s,p}(T, C)$$

$$\varepsilon_{e,n} = \varepsilon_{e,n}(T, C)$$

$$\varepsilon_{e,p} = \varepsilon_{e,p}(T, C)$$

$$\varepsilon_{e,s} = \varepsilon_{e,s}(T, C)$$

$$\varepsilon_{s,n} = \varepsilon_{s,n}(T, C)$$

$$\varepsilon_{s,p} = \varepsilon_{s,p}(T, C)$$

Each parameter is described by a 2-D lookup table (3 current breakpoints *4 temperature breakpoints) with discharge current rate and temperature as inputs, and the model parameter is the output. Internally, each parameter is evaluated by a linear interpolation method according to two inputs. The fidelity of the model can be improved by increasing the number of points related to discharge current rate and temperature, but introducing more breakpoints can also create two problems. First, introducing more points can increase the computational cost. Second, the benefit of introducing more points is diminishing, and an excessive number of breakpoints may generate numerous parameter values that are not consistent with the optimal solutions [24].

2.3. Sensitivity analysis of model parameters

Sensitivity analysis involves local and global sensitivity analysis. In this paper, to remove the redundant parameters and adjust the model, local sensitivity analysis is employed, and the coupled effects of two parameters are not considered. The output voltage curves, which replace the sensitivity factor, are adopted to describe the parameter sensitivity because a slight change in the seven characteristic parameters may greatly influence the output. In local sensitivity analysis, the specific input parameter is changed slightly around the nominal value, and the responses of the model output are compared [25].

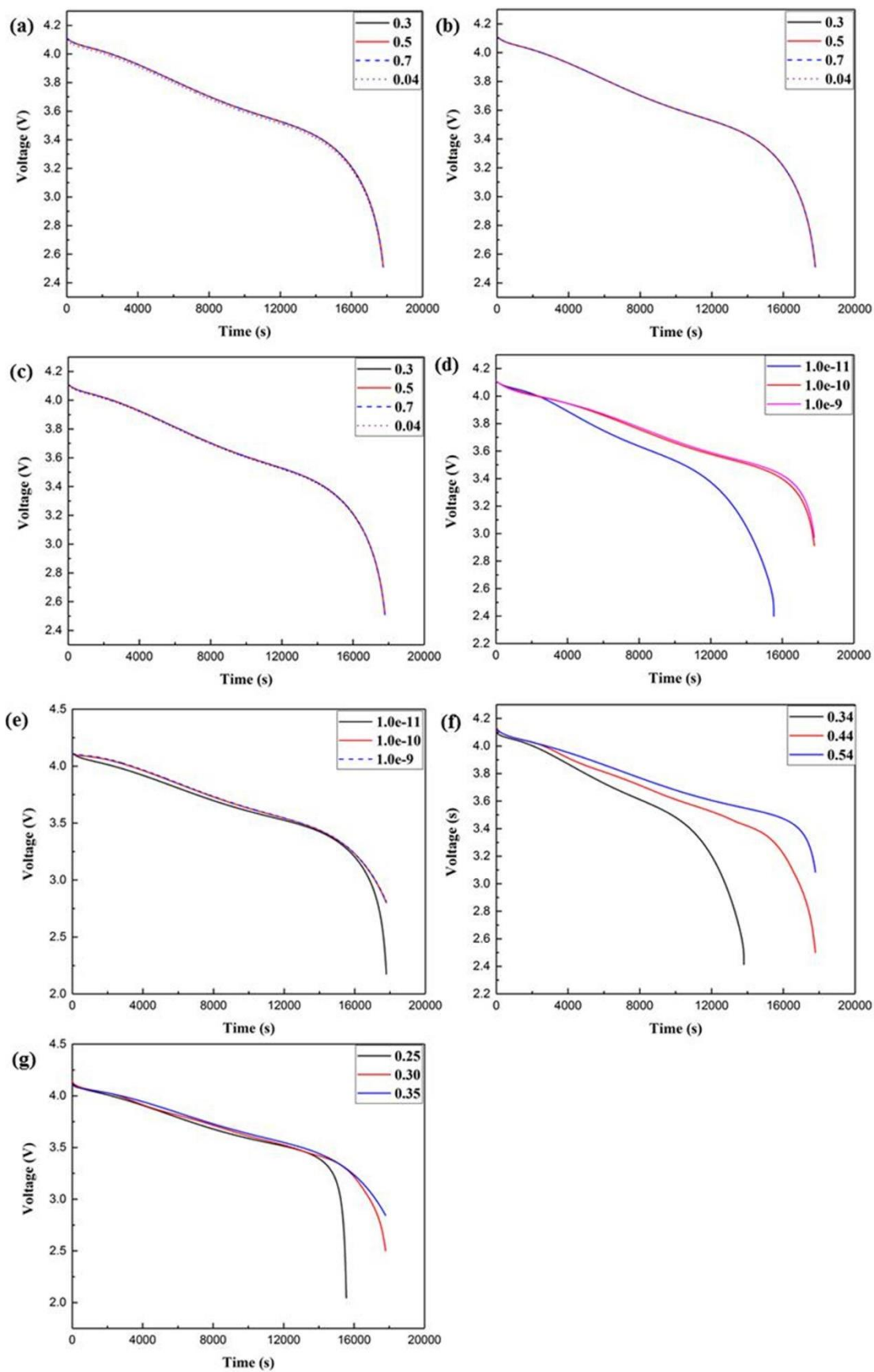


Figure 4. Sensitivity analysis of model parameters (a) $\epsilon_{e,n}$, (b) $\epsilon_{e,p}$, (c) $\epsilon_{e,s}$, (d) $D_{s,n}$, (e) $D_{s,p}$, (f) $\epsilon_{s,n}$, and (g) $\epsilon_{s,p}$.

Figure 4a-c shows the sensitivity analysis curves of $\epsilon_{e,n}$, $\epsilon_{e,p}$ and $\epsilon_{e,s}$ separately, and their input parameters are all varied with a fixed step size of 0.2. Even when the input parameter is sharply decreased to 0.04, the output curves are all anastomotic, which indicates that the three parameters are insensitive. The sensitivity analysis curves of $D_{s,n}$ and $D_{s,p}$ are shown in Figure 4d and e. The input values are set to $1.0\text{e-}11$, $1.0\text{e-}10$ and $1.0\text{e-}9$ separately because of the broad value range relative to the order of magnitude. Figure 4f-g shows the sensitivity analysis curves of $\epsilon_{s,n}$ and $\epsilon_{s,p}$. Their fixed step sizes are 0.1 and 0.05, respectively. As shown in Figure 4d-g, the output curves vary greatly, especially at the end of discharge, which demonstrates that the four parameters are sensitive parameters and that slight changes in their values can greatly influence the model's fidelity. Therefore, $\epsilon_{e,s}$ is selected from three insensitive parameters and assigned an optimal value of 0.30446, which is identified by GA at 25°C.

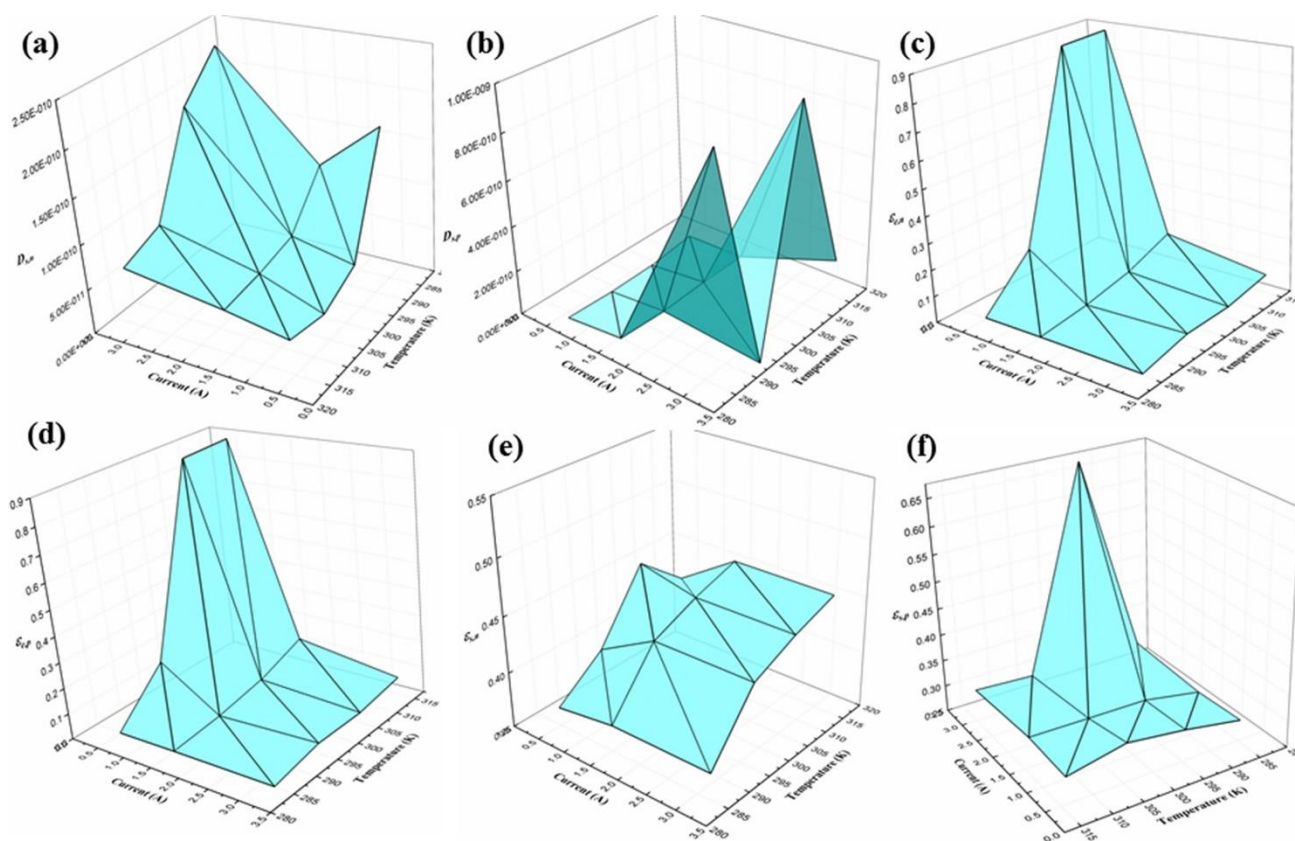


Figure 5. Fitting surfaces of the model parameters (a) $D_{s,n}$, (b) $D_{s,p}$, (c) $\epsilon_{e,n}$, (d) $\epsilon_{e,p}$, (e) $\epsilon_{s,n}$, and (f) $\epsilon_{s,p}$.

The relationships between the other model parameters, temperature and current are illustrated in Figure 5. In the negative electrode, $D_{s,n}$ (Figure 5a) and $\epsilon_{s,n}$ (Figure 5e) both increase with increasing temperature, but only $D_{s,n}$ increases appreciably with increasing current. In the positive electrode, the dependence of $D_{s,p}$ (Figure 5b) and $\epsilon_{s,p}$ (Figure 5f) on temperature and current is distinct when the current increases, showing an irregular shape with temperature. In the electrolyte phase, $\epsilon_{e,n}$ (Figure 5c) and $\epsilon_{e,p}$ (Figure 5d) show a similar dependence on temperature and current. The sensitivity analysis can not only decrease the number of 2-D lookup tables required and maintain model precision but also benefit the subsequent model calibration.

3. RESULTS AND DISCUSSION

3.1. Experimental verification

In this paper, 3.5 Ah NCM 18650-type cells are chosen to validate the simplified model and the proposed estimation method. The experiments include constant current discharge tests and two self-designed pulse current tests. A host computer for profile setting and data storage, a battery testing system (Shenzhen Neware Technology CO., LTD), a programmable fast thermal test chamber (MSK-TE906, Shengzhen Kejing Star Technology CO., LTD) and temperature sensors attached to the cells are shown in Figure 6. The cells are charged to 4.2 V by the standard constant-current constant-voltage (CCCV) scheme according to the manufacturer's guidelines and discharged to 2.5 V at different current rates (0.2C, 0.5C, 1C and 2C) and temperatures (10°C, 20°C, 30°C and 40°C). The self-designed pulse current tests include two sections, and the current profiles are shown in Figure 7a and b, respectively. One is the 1C pulse discharge test, which is implemented over the range of 20%-90% SOC in steps of 10%. To validate the adaptation of the proposed method to different charge/discharge current rates, the other is a 4-step pulsed-current test applied with a current rate of 0.2C, 0.5C, 1C and 2C. For the two pulse discharges, the temperature increase is minute and ignored because the pulse time is too short relative to the rest time. In the figures, a positive current indicates discharge, and a negative current indicates charge.

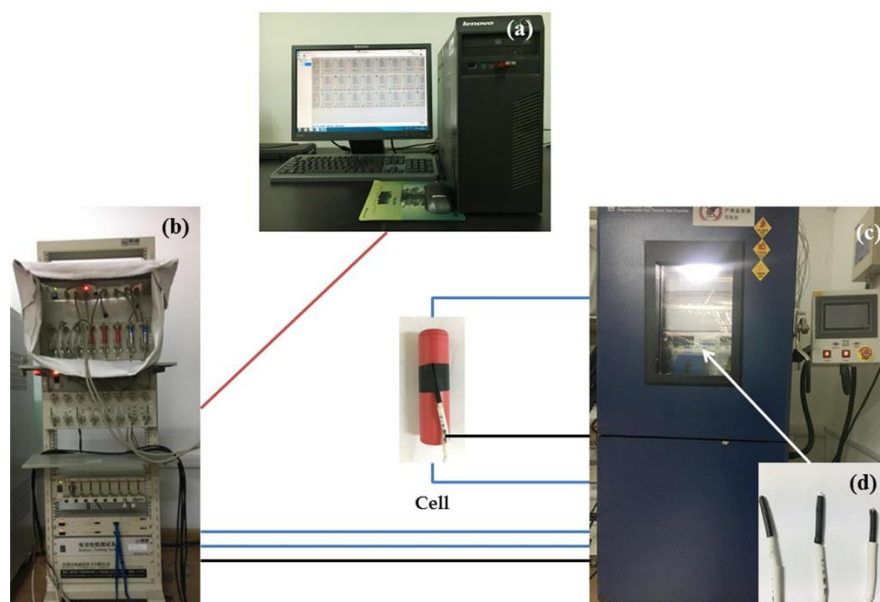


Figure 6. (a) The host computer, (b) the battery testing system, (c) the programmable fast thermal test chamber, and (d) temperature sensors.

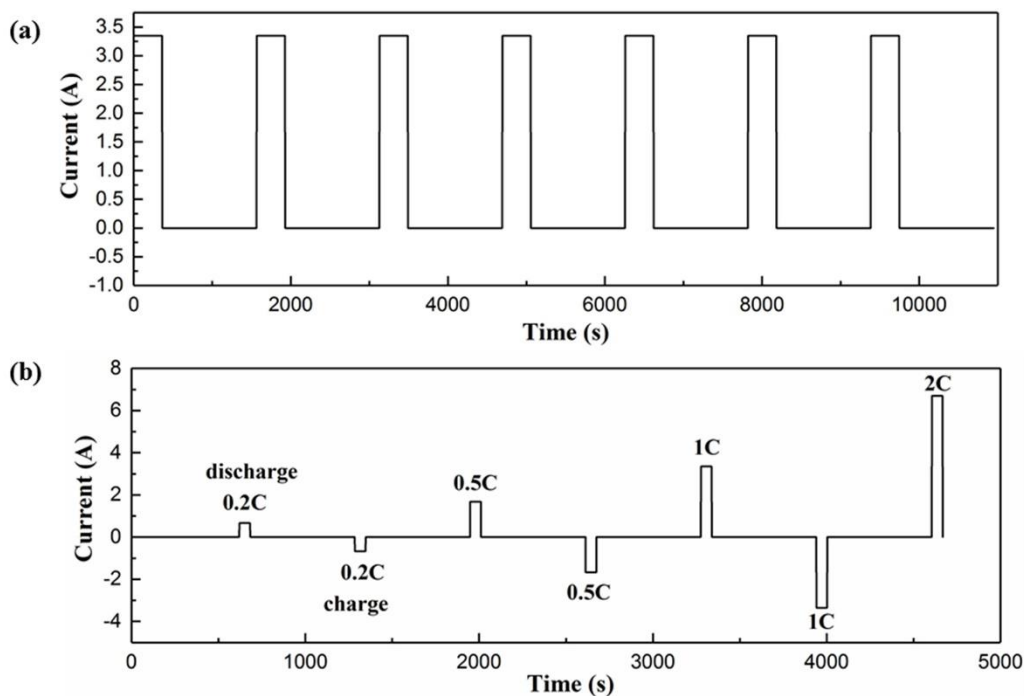


Figure 7. Current profiles of (a) 1C pulse discharge and (b) 4-step pulsed-current tests.

3.2. Algorithm validation

To verify the accuracy of the parameter identification algorithm and analyse the simplified model stability to various temperature and current effects, a comparison of the experimental and simulated terminal voltages under different temperatures and discharge rates is shown in Figure 8. Figure 8a and b describes the battery terminal voltage curves at different temperatures with a current of 0.2C and the corresponding relative error between experiment and simulation separately. The experimental and simulated curves almost overlap, and the voltage relative errors are essentially within 0.5%. The error at 25°C is slightly larger than the errors at other temperatures because the model parameters at 10, 20, 30 and 40°C are identified by the GA as breakpoints in 2-D lookup tables, but the parameters at 25°C are estimated by linear interpolation method through 2-D lookup tables. Clearly, the error is also approximately 0.5%, except at the end of discharge at 25 °C; fortunately, however, the vehicle batteries mainly operate in the middle of the SOC, which indicates that the proposed method has high fidelity and strong robustness to temperature change.

Moreover, Figure 8c and d shows the battery voltage curves and relative error under various discharge rates at 20°C. The figure illustrates that the simulated terminal voltages show excellent agreement with the experimental voltages. When the current is below 2C, the error is less than 0.5%, and when the current is up to 2C, the error still remains approximately 0.5%. Thus, the efficient but inexpensive parameter identification algorithm with 2-D lookup tables exhibits excellent performance under varying temperature and current conditions.

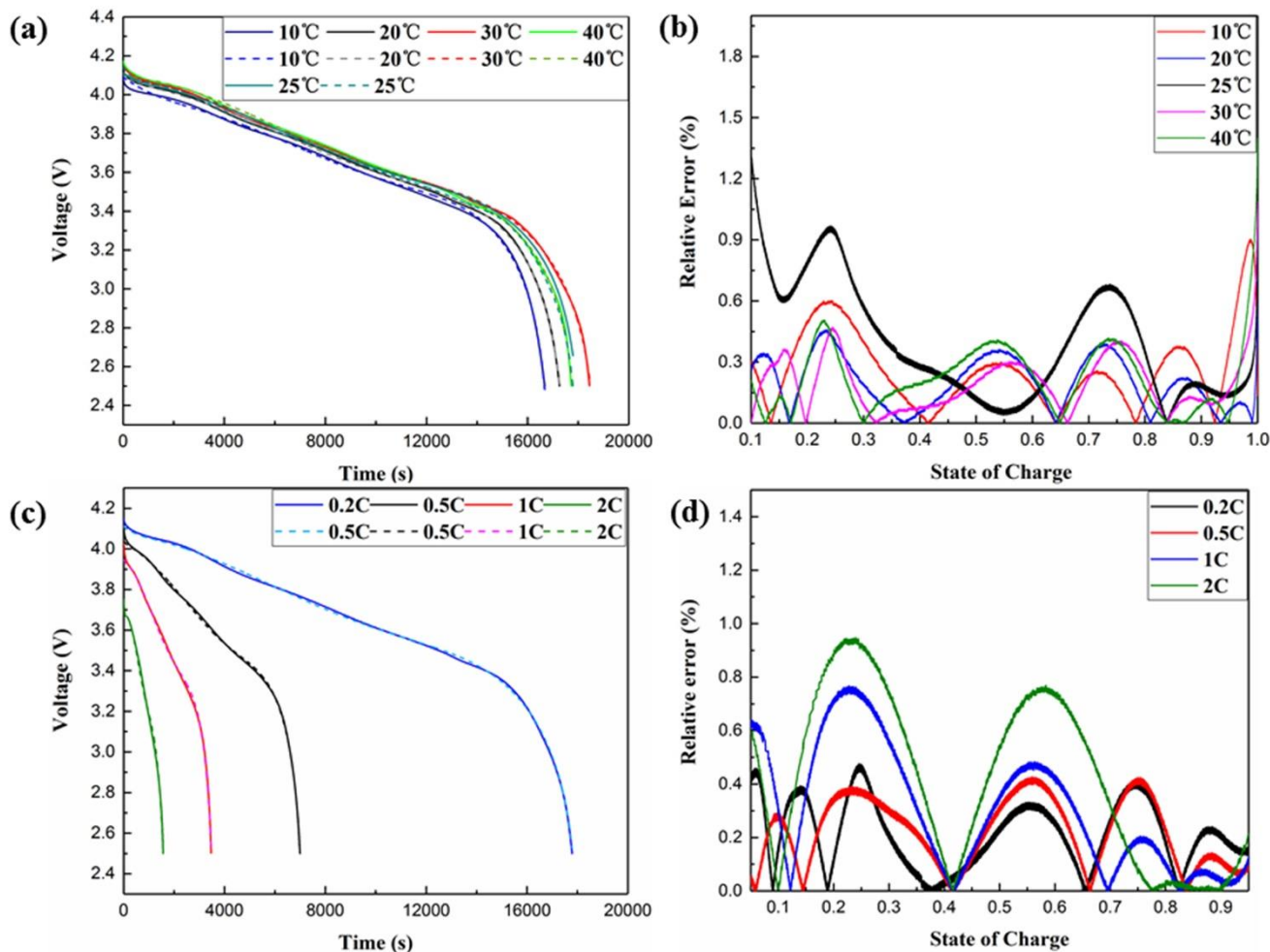


Figure 8. Comparison of experimental data and simulation results under the effects of different temperatures at 10, 20, 30 and 40°C (0.2C) (a). Relative error of temperature effect at different temperature (b) and discharge current rates 0.2, 0.5, 1 and 2C (20°C) (c). Relative error of current effect (d). ($Relative\ Error = \frac{|U_{exp} - U_{sim}|}{U_{exp}}$, the solid line is the experimental curve and the dashed line is the simulated curve).

3.3. Model validation

To verify the extracted electrochemical model with the estimated parameters, three different load profiles are implemented, including 1C discharge, 1C pulse discharge and four-step pulse discharge. The 1C discharge voltage curve at 20°C is shown in Figure 8d with a voltage error of 0~0.056 V, a relative voltage error of 0~0.7% and an average relative error of 0.2%. The corresponding simulation results and experimental data pertaining to 1C pulse discharge and four-step pulse discharge are shown in Figure 9. The simulated curve of 1C pulse discharge, which follows the experimental curve closely, increases along a straight line and then rises slowly during the rest of the period, which indicates that the simplified model simulates the voltage resilience characteristics of the battery very well. Considering Figure 8b, d and Figure 9a, it is noteworthy that the maximum estimated error appears at the end of discharge (~0.25

SOC), generally because the battery exhibits strong nonlinear characteristics at extreme SOC universally. There is good agreement between the simulated and actual charge/discharge voltages for 4 different current rates (Figure 9b), which demonstrates the excellent flexibility of the proposed model with changes in charge/discharge current rates.

Table 5. Cell voltage absolute error and simulation runtime of the three load profiles.

Load profile (20°C)	Average error voltage (mV)	Maximal error voltage (mV)	Average relative error (%)	Runtime (s)
1C discharge	11	56	0.2	0.803
1C pulse discharge	32	60	0.8	1.0
4-step pulse test	9	64	0.2	0.717

The voltage errors and simulation runtimes of the three load profiles are indicated in Table 5. The maximum voltage absolute errors for the 1C discharge, 1C pulse discharge and 4-step pulse tests are all below 65 mV, and the average relative errors are 0.2%, 0.8% and 0.2%, respectively. The simulation runtimes of the three load profiles are 0.803, 1.0 and 0.717 s, respectively, which are remarkably short and verify the simplicity and practicality of the simplified model.

The terminal voltage errors between the simulated and experimental results can be considered as the evaluation criteria for validation. Relevant studies are listed in Table 6. Parameter estimation based on lithium-ion battery models can be divided into three types: electrochemical model-based (including the work in this paper) [28-33], equivalent circuit model-based [34-37] and electrochemical/electro-thermal model-based [16, 26-27]. For the electrochemical/electro-thermal model, as shown in Table 6, temperature effects are incorporated into the parameter estimation process but the effect of current is ignored [16, 26-27]. In addition, electrochemical/electro models are coupled with a thermal model, which is quite time-consuming and complicated. Compared with the ECMs, our work shows a higher accuracy than that reported in most papers [34-37] in describing the internal phenomena of lithium-ion batteries. Furthermore, compared with other electrochemical models, the model developed in this paper considers both temperature and current as variables and estimates the model parameters online with changing temperature and current. The parameters reported in most references are identified by specific algorithms, except for those reported works [28-30], which are cited entirely. The genetic algorithm is widely applied in certain studies [26, 31] to estimate model parameters; however, our work exhibits better fidelity. Thus, compared with that reported in other studies, the cell voltage absolute error of the proposed method possesses comparatively higher accuracy and considers the effects of changing temperature and charge/discharge current rate, which are typically ignored.

Table 6. Comparison with reported works at 1C discharge

References	Model used	Algorithm	Voltage error	Temperature/current dependence
The paper	Electrochemical model	Genetic algorithm	0~0.056 V/0~0.7%/0.2%(average)	Yes
16	Electrochemical-thermal coupling model	Least-squares fit	0~0.07 V	Temperature
26	Multi-physics model	Genetic algorithm	0~0.0763 V	Temperature
27	Electrothermal model	Least-squares nonlinear algorithm	0~1%	Temperature
28	SPM	-	0~1%	Temperature
29	Simplified P2D	-	0~0.4%	No
30	Electrochemical model	-	0.2076% (average)	No
31	Electrochemical model	Genetic algorithm	0~0.1 V	No
32	Electrochemical model	Bacterial foraging optimization algorithm	0~0.08 V	No
33	Electrochemical model	Least squares	0~1%	current
34	ECM	Least-squares curve fitting	0~1.23%/0.29% (average)	Yes
35	ECM with improved P2-D model	Recursive least squares	0~0.06 V	No
36	Splice-ECM	Curve fitting	0~2%	No
37	ECM	Extend Kalman filter	0.12% (average)	No

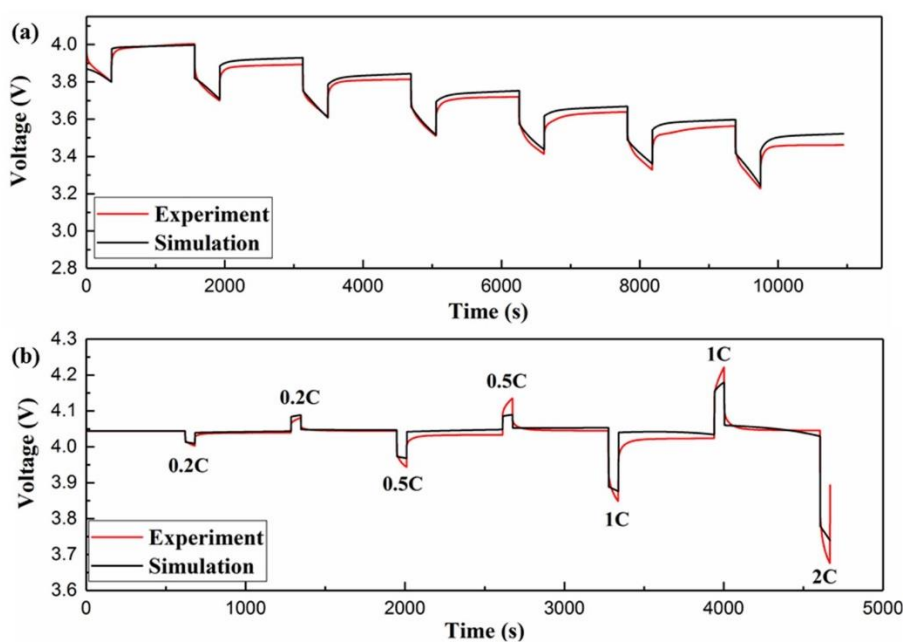


Figure 9. Comparison between experimental data and simulation results for (a) 1C pulse discharge and (b) four-step pulse tests.

In short, the flexible simplified model established by the proposed method is verified to be effective in reducing computational cost and maintaining high fidelity. The results are mainly attributed to two reasons: one is that the simplified model is greatly reduced with partial internal information loss but captures the dynamic characteristics very well, and the other is utilizing the proposed parameter identification method to relieve the influence of temperature and current on the model's performance and maintain the strong stability of the model.

4. CONCLUSION

In this paper, a simplified electrode-average model reduced using polynomial approximation and a three-variable method is proposed, which not only captures the dynamic behaviour of a battery but also simplifies the physics-based equations of the solid and electrolyte phases to reduce model complexity. A practical method is developed for identifying the model parameters employing the genetic algorithm from observed experimental data to create 2-D lookup tables with temperature and current as independent variables for online estimation. The model parameters are estimated directly for large discharge current rate, under which the temperature rises sharply during discharge. To validate the simplified model and the proposed estimation method, 3.5 Ah NCM 18650-type cells are selected. The results suggest that the simple method possesses low complexity, sufficient accuracy and excellent adaptability to changes in temperature and current rate. The simplified model combined with the proposed parameter identification method updates the parameters with a voltage error of 0~0.056 V, a relative voltage error of 0~0.7% and an average relative error of 0.2%.

ACKNOWLEDGMENTS

The research is supported by Special Funds for the Transformation of Scientific and Technological Achievements in Jiangsu Province (BA2016162), the National Science and Technology Foundation of China (2015BAG07B00), NSFC (21501071), the Six Talents Peak Project of Jiangsu Province (2016-XNYQC-003, 2015-XNYQC-008), and the Foundation for Advanced Talents of Jiangsu University (13JDG071, 12JDG054).

NOMENCLATURE

j	Reaction flux at the solid particle surface, [$\text{mol cm}^{-1} \text{s}^{-1}$]
c_s	Concentration of Li^+ ions in an electrode particle, [mol cm^{-3}]
D_s	Diffusion coefficient of lithium in an electrode particle, [$\text{cm}^2 \text{s}$]
a_s	Specific surface area of electrode, [cm^{-1}]
F	Faraday's constant, [C mol^{-1}]
ε_s	Volume fraction of region

R_i	Radius of solid particles, [cm]
σ_{eff}	Effective electronic conductivity of solid particles, [S cm ⁻¹]
ϕ_s	Solid-phase potential, [V]
A	Electrode plate area, [cm ²]
L	Total cathode-separator-anode thickness, [cm]
K^{eff}	Effective ionic conductivity of the electrolyte phase, [S cm ⁻¹]
K_D^{eff}	Effective ionic diffusional conductivity of the electrolyte phase, [S cm ⁻¹]
ε_e	Volume fraction of the electrolyte phase
C_e	Concentration of Li ⁺ ions in the electrolyte phase, [mol cm ⁻³]
t_+^0	Lithium ion transference number in the electrolyte
T	Absolute temperature, [K]
R	Universal gas constant
i_0	Exchange current density, [A cm ⁻²]
k	Intercalation/deintercalation reaction-rate constant of electrode, [A·cm ^{2.5} ·mol ^{-1.5}]
η	Overpotential, [V]
$C_{s,max}$	Maximum concentration of Li ⁺ ions in the particle of electrode, [mol cm ⁻³]
$C_{s,surf}$	Surface concentration of Li ⁺ ions in the particle of electrode, [mol cm ⁻³]
R_f	Film resistance, [Ω]
p	Positive electrode
n	Negative electrode
α_a, α_c	Anodic and cathodic transfer coefficients

References

1. L. Lu, X. Han, J. Li, J. Hua and M. Ouyang, *J. Power Sources*, 226 (2013) 272.
2. T. Dagger, P. Niehoff, C. Lurenbaum, F.M. Schappacher and M. Winter, *Energy Technology*, 6 (2018) 2023.

3. V. Ramadesigan, P. W. C. Northrop, S. De, S. Santhanagopalan, R.D. Braatz and V. R. Subramanian, Multi-scale Modeling and Simulation of Lithium-Ion Batteries from Systems Engineering Perspective, 220th ECS Meeting, Boston, America, 2011, Abstract 747.
4. K. E. Thomas, J. Newman and R. M. Darling, *Advances in Lithium-Ion Batteries*, Springer, (2002) Boston, USA.
5. J. Newman and K. E. Thomasalyea, *Electrochemical Systems*, John Wiley & Sons, (2004) Canada.
6. M. Doyle, T. F. Fuller and J. Newman, *J. Electrochem. Soc.*, 140 (1993) 1526.
7. S. De, B. Suthar, D. Rife, G. Sikha and V. R. Subramanian, *J. Electrochem. Soc.*, 160 (2013), A1675.
8. D. D. Domenico, A. Stefanopoulou and G. Fiengo, *J. Dyn. Syst. Meas. Control*, 132 (2010) 768.
9. L. Cai and R. E. White, *J. Electrochem. Soc.*, 156 (2009) A154.
10. C. Yuan, B. Wang, H. Zhang, L. Chen and H. Li, *Int. J. Electrochem. Sci.*, 13 (2018) 1131.
11. M. Chen and G. A. Rincon-Mora, *IEEE T. Energy Convers.*, 21 (2006) 504.
12. A. Jossen, *J. Power Sources*, 154 (2006) 530.
13. S. Yuan, L. Jiang, C. Yin, H. Wu and X. Zhang, *J. Power Sources*, 352 (2017) 245.
14. W. Shen, H. Li, *Energies*, 10 (2017) 432.
15. J. C. Forman, S. J. Moura, J. L. Stein and H. K. Fathy, *J. Power Sources*, 210 (2012) 263.
16. J. Li, L. Wang, C. Lyu, H. Wang and X. Liu, *J. Power Sources*, 307 (2016) 220.
17. T. S. Dao, C. P. Vyasrayani and J. Mcphee, *J. Power Sources*, 198 (2012) 329.
18. V. R. Subbramanian, V. D. Diwakar and D. Tapriyal, *J. Electrochem. Soc.*, 150 (2005) A2002.
19. Y. Ji, Y. Zhang and C. Wang, *J. Electrochem. Soc.*, 160 (2013) A636.
20. X. Han, M. Ouyang, L. Lu and J. Li, *J. Power Sources*, 278 (2015) 814.
21. S. K. Rahimian, S. Rayman and R. E. White, *J. Power Sources*, 224 (2013) 180-194.
22. T. R. Ashwin, A. MCGordon, W. D. Widanage and P. A. Jennings, *J. Power Sources*, 341 (2017) 387.
23. C. Wang, T. He, X. Liu, S. Zhong, W. Chen and Y. Feng, *Magn. Reson. Med.*, 73 (2015) 865.
24. R. A. Jackey, G. L. Plett and M. J. Klein, *SAE World Congress & Exhibition*, Detroit, USA, 2009, SAE paper 2009-01-1381.
25. T. Turányi and A. S. Tomlin, *Analysis of Kinetic Reaction Mechanisms*, Springer, (2014) Berlin Heidelberg, Germany.
26. L. Zhang, L. Wang, G. Hinds, C. Lyu, J. Zheng and J. Li, *J. Power Sources*, 270 (2014) 367.
27. S. N. Motapon, A. Lupien-Bedard, L. A. Dessaint, H. Fortin-Balanchette and K. Al-Haddad, *IEEE T. Ind. Electron.*, 64 (2017) 998.
28. T. R. Tanim, C. D. Rahn and C. Y. Wang, *J. Dyn. Syst. Meas. Control*, 137 (2014) 011005.
29. P. Kemper, S. E. Li and D. Kum, *J. Power Sources*, 286 (2015) 510.
30. N. Lotfi, R. G. Landers, J. Li and J. Park, *IEEE T. Contr. Syst. T.*, 25 (2017) 1217.
31. X. Xu, W. Wang and L. Chen, *J. Electrochem. Soc.*, 163 (2016) A1429.
32. Y. Ma, J. Ru, M. Yin, H. Chen and W. Zheng, *J. Appl. Electrochem.*, 46 (2016) 1119.
33. G. K. Prasad and C. D. Rahn, *J. Power Sources*, 232 (2013) 79.
34. Y. Zhang, Y. Shang, N. Cui and C. Zhang, *Energies*, 11 (2018) 19.
35. X. Zhang, J. Lu, S. Yuan and X. Zhou, *J. Power Sources*, 345 (2017) 21.
36. S. Wang, C. Fernandez, X. Liu, J. Su and Y. Xie, *Meas. Control-Uk*, 51 (2018) 125.
37. X. Zhang, Y. Wang, D. Yang and Z. Chen, *Energy*, 115 (2016) 219.